The Cryosphere, 6, 1463–1481, 2012
www.the-cryosphere.net/6/1463/2012/
doi:10.5194/tc-6-1463-2012

The Cryosphere

Calibration of a surface mass balance model for global-scale applications

R. H. Giesen and J. Oerlemans

Institute for Marine and Atmospheric research Utrecht, Utrecht University, Utrecht, The Netherlands

Correspondence to: R. H. Giesen (r.h.giesen@uu.nl)

Received: 22 March 2012 – Published in The Cryosphere Discuss.: 16 April 2012
Revised: 16 October 2012 – Accepted: 12 November 2012 – Published: 7 December 2012

Abstract. Global applications of surface mass balance models have large uncertainties, as a result of poor climate input data and limited availability of mass balance measurements. This study addresses several possible consequences of these limitations for the modelled mass balance. This is done by applying a simple surface mass balance model that only requires air temperature and precipitation as input data, to glaciers in different regions. In contrast to other models used in global applications, this model separately calculates the contributions of net solar radiation and the temperature-dependent fluxes to the energy balance. We derive a relation for these temperature-dependent fluxes using automatic weather station (AWS) measurements from glaciers in different climates. With local, hourly input data, the model is well able to simulate the observed seasonal variations in the surface energy and mass balance at the AWS sites. Replacing the hourly local data by monthly gridded climate data removes summer snowfall and winter melt events and, hence, influences the modelled mass balance most on locations with a small seasonal temperature cycle. Modelled winter mass balance profiles are fitted to observations on 82 glaciers in different regions to determine representative values for the multiplication factor and vertical gradient of precipitation. For 75 of the 82 glaciers, the precipitation provided by the climate dataset has to be multiplied with a factor above unity; the median factor is 2.5. The vertical precipitation gradient ranges from negative to positive values, with more positive values for maritime glaciers and a median value of 1.5 mm a^{-1} m^{-1}. With calibrated precipitation, the modelled annual mass balance gradient closely resembles the observations on the 82 glaciers, the absolute values are matched by adjusting either the incoming solar radiation, the temperature-dependent flux or the air temperature. The mass balance sensitivity to changes in temperature is particularly sensitive to the chosen calibration method. We additionally calculate the mass balance sensitivity to changes in incoming solar radiation, revealing that widely observed variations in irradiance can affect the mass balance by a magnitude comparable to a 1 °C change in temperature or a 10 % change in precipitation.

1 Introduction

The application of a glacier mass balance model on a global scale is a challenging exercise. Glaciers are situated in a variety of climates, from warm and wet to cold and dry and with seasonal cycles in temperature and/or humidity. Since the dominant processes in the surface energy and mass balance differ amongst these climates, a model should resolve all these processes for an accurate simulation of all glaciers. On the other hand, the detailed input data required for such simulations are simply not available. Meteorological measurements in mountainous terrain are scarce and suffer from local effects, whereas the spatial resolution of global and regional climate models is too coarse to resolve the specific weather conditions on glaciers. Furthermore, surface mass balance models can only be calibrated and validated on a limited sample of the world's glaciers, where meteorological and mass balance measurements have been done.

Despite these limitations, globally applied mass balance models are needed for producing estimates of the glacier contribution to sea-level rise in the next centuries. Due to the large uncertainty in meteorological data for mountainous regions, changes in the surface mass balance are generally

computed with simple models, only requiring air temperature and precipitation as climatic input data (Raper and Braithwaite, 2006; Radić and Hock, 2011; Slangen et al., 2012). Climate data is often used at a low temporal (e.g., monthly) resolution, either limited by the temporal resolution of the input data or to keep the modelling time within feasible limits. Model calibration commonly relies on the available mass balance measurements. These have only been acquired at a small number of glaciers, with the longest series for the European Alps and Scandinavia and limited data for heavily glacierised regions like the Himalaya or Alaska (Zemp et al., 2008).

In this paper, we explore the applicability of a surface mass balance model in different climatic regions. The model only requires air temperature and precipitation as input data. The surface energy balance is separated into a contribution by net solar radiation and a contribution by the fluxes dependent on air temperature. In contrast to models that only use air temperature data to calculate ablation, the model used here includes the effect of the seasonal cycle in insolation (which is generally asynchronous to the annual temperature cycle) on surface melt. The model parameters are derived from automatic weather station records from different climatic regions.

We address several issues encountered when applying a mass balance model to regions with limited availability of meteorological measurements and mass balance data. We investigate the dependence of the results on the temporal resolution of the input data by comparing results obtained with hourly and monthly temperature data. By substituting the locally measured input data by climate data from the nearest grid point, we demonstrate the potential errors introduced by using meteorological data from outside the glacier environment. Next, available altitudinal profiles of winter mass balance are used to estimate the vertical precipitation gradient and a precipitation multiplication factor for 82 glaciers in different regions. The measured annual mass balance profile is matched by calibrating three different model parameter sets. Finally, the mass balance sensitivity to changes in air temperature, precipitation and atmospheric transmissivity is assessed for the sample of 82 glaciers. Special attention is given to the effect of the parameter calibration on the calculated sensitivities.

2 Mass balance model

Model description

The mass balance model is an adapted version of the simplified mass balance model described in Oerlemans (2001, p. 48). The annual surface mass balance (B) is given by

$$B = \int_{\text{year}} \left\{ P_{\text{snow}} + (1-r)\min\left(0;\ -\frac{Q}{\rho_{\text{w}} L_{\text{f}}}\right)\right\} \mathrm{d}t, \qquad (1)$$

Table 1. Values for the fixed model parameters. The values for the parameters calibrated at the AWS sites are listed in Table 2.

Parameter	Symbol	Value	Unit
Latent heat of fusion	L_{f}	3.34×10^5	J kg^{-1}
Water density	ρ_{w}	1000	kg m^{-3}
Ice density	ρ_{ice}	900	kg m^{-3}
Specific heat capacity of ice	c_{ice}	2090	$\text{J kg}^{-1}\,\text{K}^{-1}$
Fresh snow albedo	α_{frsnow}	0.69–0.90	–
Firn albedo	α_{firn}	0.55	–
Albedo time-scale	t_*	21.9	days
Albedo depth-scale	d_*	0.001	m w.e.
Depth of subsurface layer	δz	2.0	m
Threshold temperature for snow	T_{snow}	1.5	°C
Temperature lapse rate	Γ	0.0065	K m^{-1}

with mass gain resulting from solid precipitation P_{snow} and mass loss determined from the surface energy balance Q. Precipitation falls as snow when the air temperature is below a threshold temperature T_{snow}. Melt is assumed to occur whenever the surface energy balance is positive and part of the meltwater r is allowed to refreeze within the snowpack. The constant L_{f} is the latent heat of fusion, ρ_{w} is the water density (Table 1).

The energy available for melt at the surface is determined from a simplified representation of the surface energy balance, calculated at hourly time-steps. Because accurate humidity, cloudiness and wind speed data are rarely available for glacierised areas, the model is set up in such a way that it only requires air temperature and precipitation data as input. Since net solar radiation is not an explicit function of air temperature, it is treated separately from the other fluxes in the energy balance, which are directly dependent on air temperature. Hence, the surface energy balance is divided into two terms (Oerlemans, 2010, p. 100):

$$Q = (1-\alpha)\,\tau\, S_{\text{in,TOA}} + \psi \qquad (2)$$

where the first term describes the net solar radiative flux and the second term represents all other atmospheric fluxes, dependent on air temperature T_{a}.

Net solar radiation is computed by multiplying the incoming solar radiation at the top of the atmosphere ($S_{\text{in,TOA}}$) by the atmospheric transmissivity τ and subtracting the part of the incoming solar radiation reflected by the surface with albedo α. The atmospheric transmissivity represents all processes that affect solar radiation from the top of the atmosphere to the glacier surface, including attenuation by scattering and absorption in the clear-sky atmosphere, the transmission of radiation through clouds and shading by the topography. $S_{\text{in,TOA}}$ is computed from standard astronomical relations (e.g. Iqbal, 1983), for τ we use one value without seasonal variation. For studies of individual glaciers, τ can be calculated in a more sophisticated way, but for global applications, the required input data (e.g., cloud observations, topography) are generally not available. When no snow is

Table 2. Values for the model parameters τ, α_{ice}, c ($W\,m^{-2}\,K^{-1}$), ψ_{min} ($W\,m^{-2}$) and T_{tip} (°C), calibrated for the individual AWS sites. The standard values used in the global application of the model are also listed. The values for the other model parameters are listed in Table 1.

Data set	Short name	τ	α_{ice}	c	ψ_{min}	T_{tip}
AWS site						
Vadret da Morteratsch	Mort	0.47	0.25	12.0	−26	+4.1
Glaciar Lengua	Leng	0.32	0.20	28.0	–	–
Midtdalsbreen	Midt	0.54	0.35	8.7	−25	−1.5
Storbreen	Stor	0.48	0.35	8.4	−19	+0.2
Breidamerkurjökull	Brei	0.44	0.15	22.6	−23	+0.9
S5 Greenland	GrS5	0.55	0.55	37.4	−26	+2.3
S6 Greenland	GrS6	0.63	0.55	40.5	−31	+1.1
Belcher Glacier	Belch	0.62	0.45	19.1	−42	+4.1
Kongsvegen	Kong	0.55	0.35	10.8	−33	−0.8
Standard						
Small c	set1	0.50	0.35	10.0	−25	+1.0
Large c	set2	0.50	0.35	30.0	−25	+1.0

present, a constant ice albedo is used. After a snowfall event, α decreases exponentially from the fresh snow albedo α_{frsnow} to the firn albedo α_{firn}, controlled by the time-scale t_* (Oerlemans and Knap, 1998). For small snow depths, α is a function of both snow and ice albedo, according to the depth-scale d_*. The fresh snow albedo is lowered for snowfall events at temperatures around the melting point by making α_{frsnow} dependent on the air temperature during snowfall (Giesen and Oerlemans, 2010).

The temperature-dependent energy fluxes are represented by a function ψ derived from measurements at weather stations on 11 glaciers in different climates (Fig. 1, Appendix A):

$$\psi = \begin{cases} \psi_{min} + c\,T_a & \text{for } T_a \geqslant T_{tip}; \\ \psi_{min} & \text{for } T_a < T_{tip}. \end{cases} \quad (3)$$

Hence, for air temperatures below a threshold temperature T_{tip}, ψ has a constant value ψ_{min}. For higher temperatures, ψ increases linearly with T_a, the rate of increase given by c. Representative values for ψ_{min}, c and T_{tip} for the non-tropical AWS sites are given in Table 2.

When the right-hand side of Eq. (2) is positive, meltwater is formed. In case the surface consists of ice, the water runs off immediately. If snow is present, a fraction r of the meltwater refreezes and heats the snowpack, while the remaining meltwater runs off. Following Oerlemans (1991), r depends on the subsurface layer temperature T_{sub} (in °C):

$$r = 1 - \exp\{T_{sub}\}. \quad (4)$$

The change in T_{sub} resulting from refrozen meltwater is calculated as

$$\frac{dT_{sub}}{dt} = \frac{r\,Q}{\rho_{ice}\,c_{ice}\,\delta z}, \quad (5)$$

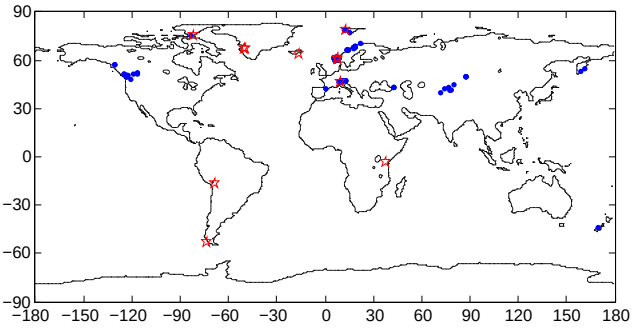

Fig. 1. Locations of the AWS sites (red stars, Table 5) and the 82 glaciers with winter and annual mass balance profiles (blue dots, Supplement).

where ρ_{ice} is ice density, c_{ice} the specific heat capacity of ice and δz the subsurface layer depth (Table 1). At the end of the summer season (here defined as calendar day 21 (1 May) in the Southern and 305 (1 November) in the Northern Hemisphere), T_{sub} is reset to the annual mean air temperature. If this temperature is higher than the melting point, T_{sub} is set to the melting point and refreezing will not occur at this location. This simplification of the refreezing process was shown to provide a good approximation of superimposed ice formation calculated with a sophisticated snowpack model (Wright et al., 2007).

3 Meteorological input data

In this section, the three different meteorological input datasets are described. The first two datasets are used to determine values for the model parameters and to examine the model performance at the AWS sites. The gridded data is additionally used in the global application of the mass balance model.

3.1 Hourly AWS data

The applicability of the albedo routine and the relation for ψ at the different AWS locations was examined using incoming solar radiation and air temperature measured by the AWS as model input. By using the most accurate input data available, it was possible to validate the parameterisations by a comparison of the measured and simulated seasonal cycles of net solar radiation and ψ. The meteorological records from Glaciar Lengua and Belcher Glacier are too short to be included in the analysis. For each of the other sites, a representative value for α_{ice} was determined from measured ice albedo (Table 2). These values correspond to the local surface characteristics and are partly determined by the location of the AWS with respect to the equilibrium line and the glacier tongue. Annual precipitation $P_{ann,AWS}$ (Table 3) was distributed equally over the year and chosen such that the modelled snow depth at the beginning of the ablation season (1 May) matched the

Table 3. Annual mean air temperature (T_{ann}), diurnal temperature range ($T_{range,AWS}$) and annual precipitation (P_{ann}) calculated from the AWS and CRU data. The annual precipitation at the AWS site ($P_{ann,AWS}$) is derived as described in the text. The CRU values are given for the gridpoint elevation (z_{CRU}), before applying the temperature lapse rate or the precipitation multiplication factor p.

AWS site	$T_{ann,AWS}$ (°C)	$T_{range,AWS}$ (°C)	$P_{ann,AWS}$ (m)	$T_{ann,CRU}$ (°C)	$T_{range,CRU}$ (°C)	$P_{ann,CRU}$ (m)	p –	z_{CRU} (m a.s.l.)
Vadret da Morteratsch	+1.6	6.5	2.4	−1.8	5.1	1.5	1.8	2676
Midtdalsbreen	−1.4	4.2	3.1	−2.6	5.2	1.2	2.1	1514
Storbreen	−1.9	4.3	2.6	−2.9	5.5	1.0	2.1	1466
Breidamerkurjökull	+2.0	4.1	1.7	+1.6	5.3	1.8	0.0	294
S5 Greenland	−5.5	4.9	0.5	−6.5	9.1	0.3	0.2	333
S6 Greenland	−10.7	6.6	0.4	−9.1	8.9	0.4	0.7	825
Kongsvegen	−9.0	4.2	1.0	−8.8	4.9	0.5	1.9	563

measured accumulation. This allowed us to compare modelled and measured ablation in the main melt season.

3.2 Monthly AWS data

The effect of the temporal variability in the input data on the modelled mass balance was investigated by using mean seasonal cycles for air temperature and diurnal temperature range. These are based on monthly mean values computed from the AWS data, averaged over all years in each record. The daily temperature cycle was prescribed as a sine function, with the amplitude determined by the monthly mean daily temperature range. Incoming solar radiation was calculated from $S_{in,TOA}$ and a constant value of τ, computed as the ratio of the annual sums of measured incoming solar radiation and $S_{in,TOA}$ (Table 2). For precipitation, we used the same annual value as for the hourly AWS data.

3.3 Monthly gridded global climate data

To calculate surface mass balances on a global scale, we used a high-resolution (10′) dataset of air temperature, diurnal temperature range and precipitation from the Climate Research Unit, University of East Anglia (CRU CL 2.0, New et al., 2002), hereafter referred to as CRU data. This dataset is based on measurements at a large number of weather stations, interpolated to a regular grid with a spline-fitting technique. This method takes into account the latitude, longitude and elevation of the weather stations and grid cells. However, surface properties are not considered, which could lead to large air temperature deviations where land station data are interpolated over ice caps and ice sheets. Data is available for all land areas outside Antarctica. We used the average monthly values for the period 1961–1990. Incoming solar radiation was computed in the same way as for the monthly AWS data.

For the simulations at the AWS locations, we extracted the CRU seasonal cycles of air temperature, daily temperature range and precipitation from the nearest gridpoint. The gridpoint elevations differ by −157 m (S5 Greenland) to +561 m (Vadret da Morteratsch) from the AWS site altitudes. Air temperature was extrapolated to the AWS elevation with a constant temperature lapse rate Γ (Table 1). To obtain realistic accumulation at the beginning of the ablation season, we multiplied the CRU precipitation with a factor p (Table 3).

For the simulations on the global grid, the same temperature lapse rate Γ was used. Precipitation was extrapolated using two parameters; subsequent to multiplying the CRU precipitation by a factor p, we applied a linear increase in precipitation with altitude γ:

$$P_{ann}(z) = p\, P_{ann,CRU} + \gamma\, (z - z_{CRU})\,. \quad (6)$$

4 Seasonal cycles at the AWS sites

The seven AWS sites cover a considerable range in climates, from an alpine climate with ablation dominated by solar radiation to a maritime climate with ablation all year round and an arctic climate with numerous snowfall events during summer. Since differences between the input datasets may affect the modelled mass balance, we shortly discuss the mean seasonal cycles of air temperature, diurnal temperature range and precipitation from the AWS and CRU data (Fig. 2). As the climatic conditions at Midtdalsbreen and S6 are similar to Storbreen and S5, respectively, these are not shown separately.

For Vadret da Morteratsch, Storbreen and Kongsvegen, the CRU temperatures correspond reasonably well with the AWS temperatures. Winter temperatures for Storbreen are lower in the CRU dataset, probably because weather stations are generally located in valleys where the air is less well mixed than on the glacier. Summer air temperatures for Kongsvegen are higher in the CRU data set, this could be due to local effects or the different measurement periods of the two datasets. For Breidamerkurjökull and S5 on Greenland, the seasonal temperature cycle is considerably larger in the CRU dataset. Like on Storbreen, the air on the glacier is probably better mixed in winter, while it is katabatically cooled in summer. The diurnal temperature range in the CRU dataset corresponds reasonably well with the AWS measurements on Vadret da

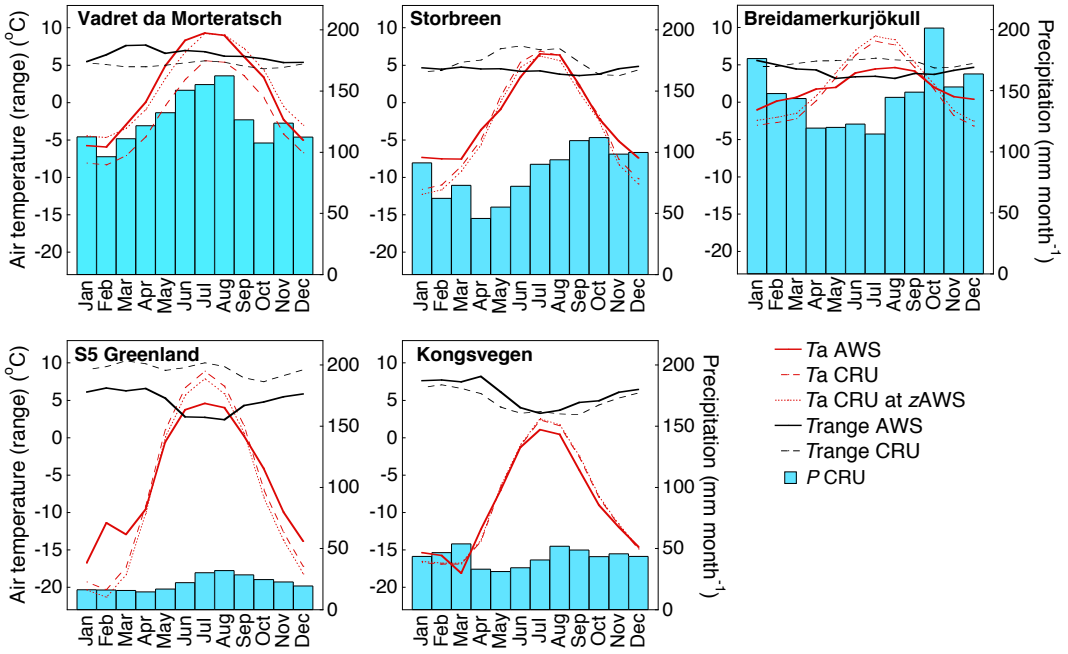

Fig. 2. Seasonal cycles of air temperature and diurnal temperature range from the AWS measurements and CRU data and precipitation from the original CRU dataset. To facilitate comparison, the temperature data from CRU have been extrapolated to the elevation of the AWS site using a lapse rate of $0.0065\,\mathrm{K\,m^{-1}}$.

Morteratsch and Kongsvegen, while it is considerably higher on the other three glaciers, especially in summer. Some of the small differences between the seasonal cycles are probably due to the different periods covered by the AWS records and the CRU dataset, while the large discrepancies are more likely caused by the local setting of the measurement sites.

We performed model simulations for each of the AWS sites, using the three meteorological input datasets described in the previous section: AWS hour, AWS month and CRU. The calculations with AWS input data were carried out with values for τ, α_{ice}, c, ψ_{min} and T_{tip} calibrated for the particular sites (Table 2). With the CRU input data, three simulations were performed to examine the effect of the parameter values on the energy and mass balance. One simulation was done with the same parameter values as the runs with the AWS input data. The second and third runs were performed with two sets of standard values also used in the global simulations (set1 and set2, Table 2), with different values for c representing the range of values found for the AWS sites (10.0 and $30.0\,\mathrm{W\,m^{-2}\,K^{-1}}$, respectively). Measured and modelled seasonal cycles of net solar radiation, temperature-dependent flux and cumulative mass balance are shown in Fig. 3. Note that net solar radiation provides the majority of the melt energy at all locations and that the maximum contributions by net solar radiation and the temperature-dependent fluxes do not coincide at most of the AWS sites.

The simulations with hourly AWS data were carried out over all complete mass balance years (starting 1 October) with available data. Subsequently, the mean seasonal cycle was computed by averaging over all years for each calendar day, where the number of years varies for the different locations (Table 5). With these realistic input data, the model is generally well able to capture the measured seasonal cycles in the energy fluxes.

Although we used measured incoming shortwave radiation for these simulations, net solar radiation depends on the albedo generated by the model. At all locations, modelled net solar radiation closely follows the measurements, demonstrating that the transition from snow to ice albedo is well represented in the model. Net solar radiation is too small in May for Vadret da Morteratsch, which is a direct result of the later disappearance of the snow cover in the model. On Kongsvegen, the variability in surface albedo and, hence, net solar radiation is difficult to model correctly. The AWS is situated approximately at the equilibrium-line altitude, where interannual variations in winter precipitation lead to net accumulation in some years and net ablation in others. Furthermore, frequent summer snowfalls cause large variability in the albedo. As we use the same amount of precipitation in each year, distributed equally over all days, the model cannot reproduce this variability.

Differences between the modelled and measured temperature-dependent fluxes are largest in spring. Although air temperatures are similar in spring and autumn, weather conditions are generally less humid, cloudy and windy in spring than in autumn. Both situations cannot be captured with a parameterisation that depends on air temperature alone. Still, a significant part of the variations in measured

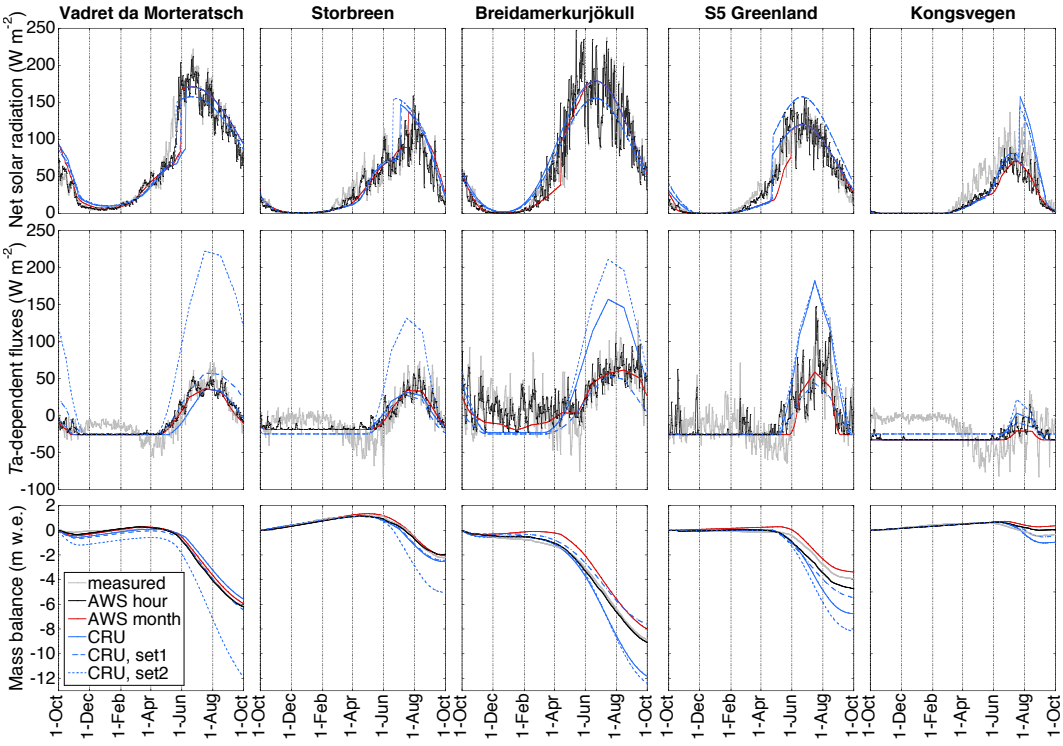

Fig. 3. Measured and modelled net solar radiation, temperature-dependent flux and mass balance at five AWS sites, using the three input datasets and calibrated model parameters. For the CRU input data, two simulations with standard values for τ, α_{ice} and c are also shown.

ψ are reproduced with the model, indicating that using only temperature does not result in a large reduction of the variability.

Since we use a constant precipitation function, the build-up of the winter snowpack deviates from the observations at most locations. Despite these deviations, the onset of melt and the melt rate in summer correspond very well with the measurements. In general, we can conclude that the model parameterisations for surface albedo and ψ are applicable in this variety of climates.

When the input data is simplified to monthly AWS temperature data and calculated incoming solar radiation, the interdaily variations disappear, but the overall shape of the seasonal cycles remains. At Breidamerkurjökull, S5 on Greenland and Kongsvegen, ablation events on warm days in winter and spring are not captured with the monthly data and the mass balance is less negative than observed. The summer melt rate is less sensitive to interdaily variations in temperature and is similar to the results obtained with hourly AWS input data at all sites.

Deviations from the measured seasonal cycles become larger when CRU data is used, especially for Breidamerkurjökull and S5 on Greenland. Since solar radiation is treated the same as with monthly AWS data, this is entirely the effect of the temperature input data. For these locations, the annual temperature cycle at the nearest CRU gridpoint is larger than measured at the AWS site (Fig. 2). In the summer months, temperatures are overestimated by 2 to 4 °C, which together with the large values for c lead to much larger temperature-dependent fluxes than measured. Too low winter temperatures at Breidamerkurjökull inhibit melting in winter, resulting in a best match with observed winter mass balance for $p = 0.0$ (Table 3). For Kongsvegen, the large interannual variations in the summer albedo cannot be simulated with the CRU data, resulting in an overestimation of net solar radiation and melt. Although the seasonal cycle of the temperature-dependent fluxes also differs from the measurements at Vadret da Morteratsch and Storbreen, the annual mass balance does not deteriorate considerably when CRU input data is used.

The change from calibrated to standard τ is relatively small at all AWS sites and hardly affects net solar radiation and the surface mass balance. For Breidamerkurjökull and S5 on Greenland, the change to standard α_{ice} is large and has a considerable effect on net solar radiation and the surface mass balance. Replacing calibrated temperature-dependent flux parameters by set1 gives the smallest changes on Storbreen, where all parameters are rather close to the standard values. The change in the temperature-dependent flux on Vadret da Morteratsch and Kongsvegen is mainly attributable to the different value for T_{tip}, not c. For Breidamerkurjökull and S5, the substantially lower value for c compensates for the overestimated air temperatures in the CRU data, improving the match with measured temperature-dependent

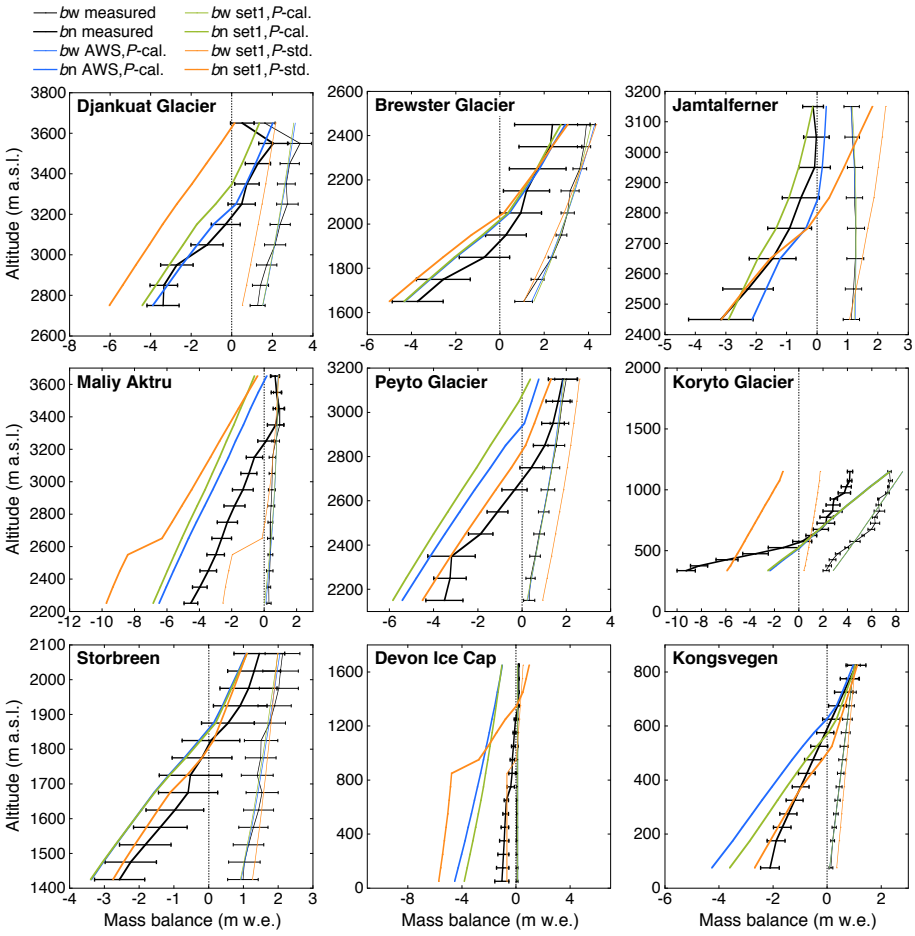

Fig. 4. Modelled and measured winter and annual mass balance profiles for glaciers in different regions (Table 4). The scales on the horizontal and vertical axes are chosen such that a 45° slope corresponds to a mass balance gradient of 1 m w.e. (100 m)$^{-1}$ in all panels. The error bars on the measured profiles represent the standard deviation over the period of measurements. Model results with precipitation parameters calibrated with the winter balance profile (P-cal.) are shown with model parameters from the most similar AWS site (AWS) and standard values (set1). A simulation with standard precipitation parameters (P-std., $p = 2.5$ and $\gamma = 1.5$ mm a^{-1} m^{-1}) and set1 is also included.

fluxes and ablation. With set2, the temperature-dependent flux barely changes for S5. For Breidamerkurjökull, the increase in ψ is balanced by a decrease in S_{net} due to the higher albedo and the mass balance for set2 is almost unchanged with regard to CRU data with calibrated parameters. The summer temperatures at the different sites clearly determine the sensitivity of the mass balance to changes in c; while the ablation increases by almost 6 m w.e. between set1 and set2 on Vadret da Morteratsch, the mass balance on Kongsvegen only changes by 0.5 m w.e. However, at both locations, this corresponds to a doubling of the surface lowering.

5 Altitudinal mass balance profiles

The precipitation multiplication factor p and the vertical gradient γ are expected to vary over the globe. Values for the two precipitation parameters were derived by a least-squares fit of the modelled to the observed winter mass balance profile for all glaciers with profiles available. Winter and annual mass balance profiles are available from the World Glacier Monitoring Service (WGMS, Haeberli et al., 2009, and earlier issues) for 82 glaciers, with a strong bias to Scandinavia and Canada (see Supplement for a table listing the 82 glaciers). For each glacier, the mean observed winter and annual balance profiles were calculated by averaging over all years with available mass balance measurements. Since the measurement date is seldomly reported for the winter balance, the mass balance calculated for 1 May (1 November on the Southern Hemisphere) is used in the fitting procedure.

Figure 4 shows the observed mass balance profiles for nine glaciers in different regions (Table 4), together with profiles simulated with calibrated (P-cal.) and standard (P-std.) precipitation parameters. The standard set of precipitation parameters was chosen in the midrange of the calibrated values: $p = 2.5$ and $\gamma = 1.5$ mm a^{-1} m^{-1}. For the other model parameters, we used the calibrated parameter set of the AWS site in

Table 4. Location (latitude, longitude), number of profiles (#), AWS parameter set, equilibrium-line altitude (ELA) and elevation of the nearest CRU grid point (z_{CRU}) for nine glaciers in different regions. Calibrated model parameters and mass balance sensitivities for all 82 glaciers can be found in the Supplement.

Glacier	Region	Latitude ° N	Longitude ° E	#	Set AWS	ELA (m a.s.l.)	z_{CRU} (m a.s.l.)
Djankuat Glacier	Caucasus	43.20	42.77	38	Mort	3213	2777
Brewster Glacier	New Zealand	−44.07	169.43	4	Stor	1923	1058
Jamtalferner	Central Europe	46.87	10.17	13	Mort	2965	2368
Maliy Aktru	Central Asia	50.08	87.75	12	Mort	3177	2747
Peyto Glacier	Coast/Rocky Mountains	51.67	−116.53	27	Mort	2720	2267
Koryto Glacier	Kamchatka	54.83	161.73	2	Stor	646	511
Storbreen	Scandinavia	61.57	8.13	16	Stor	1773	1466
Devon Ice Cap	Arctic	75.42	−83.25	3	Kong	1125	1489
Kongsvegen	Arctic	78.80	12.98	8	Kong	591	540

Table 5. Location of the AWS sites and characteristics of the records used for model calibration and validation.

Location	Latitude (° N)	Longitude (° E)	Altitude (m a.s.l.)	Period	Interval (h)	Reference
Kersten Glacier, Tanzania	−3.08	37.35	5873	09.02.05–23.01.08	1.0	Mölg et al. (2009)
Zongo Glacier, Bolivia	−16.25	−68.17	5060	28.01.05–27.01.06	0.5	Sicart et al. (2005)
Vadret da Morteratsch, Switzerland	46.42	9.93	2115	08.07.98–14.05.07	0.5	Oerlemans et al. (2009)
Glaciar Lengua, Gran Campo Nevado, Chile	−52.81	−73.00	450	23.02.00–12.04.00	1.0	Schneider et al. (2007)
Midtdalsbreen, Norway	60.57	7.47	1450	01.10.00–08.09.06	0.5	Giesen et al. (2008)
Storbreen, Norway	61.60	8.13	1570	06.09.01–11.09.06	0.5	Andreassen et al. (2008)
Breidamerkurjökull, Iceland	64.09	−16.32	190	06.05.02–06.05.06	0.5	unpublished
S5, K-transect, Greenland	67.10	−50.12	490	28.08.03–27.08.07	1.0	Van den Broeke et al. (2008)
S6, K-transect, Greenland	67.08	−49.38	1020	01.09.03–31.08.07	1.0	Van den Broeke et al. (2008)
Belcher Glacier, Devon Ice Cap, Canada	75.58	−81.43	500	02.06.08–31.07.08	1.0	unpublished
Kongsvegen, Svalbard	78.78	13.16	540	13.04.00–12.04.04	1.0	Krismer (2009)

the most similar climatic setting (Table 4). Similar to the previous section, we also show results obtained with a standard parameter set, to illustrate the effect of using different parameter values and to allow for a comparison between glaciers. A value of $c = 10.0\,\mathrm{W\,m^{-2}\,K^{-1}}$ (set1) was used, since this value generally gave good results for the AWS locations.

At most glaciers, the winter mass balance increases approximately linearly with altitude and can be fitted quite well by varying the two parameters. Repeating the fitting procedure with model parameters from set1 hardly affected the values found for p and γ, demonstrating the robustness of the fitting method and the small influence of melting on the winter balance profile.

The winter profiles modelled with standard parameters illustrate the necessity of calibrating the precipitation parameters. Reasonable agreement with the measured profiles is still obtained for Brewster Glacier, Storbreen and Kongsvegen, where the calibrated precipitation parameters are similar to the standard values. For the other glaciers, the modelled mass balance gradient and/or the absolute values of the winter balance are incorrect, resulting in large errors in the modelled annual mass balance. In the dry climates at Devon Ice Cap and Maliy Aktru, the overestimated precipitation gradient produces no solid precipitation at elevations below 850 and 2600 m a.s.l., respectively, resulting in a sudden change in the annual mass balance gradient.

With calibrated values for p and γ, the measured annual mass balance gradient is captured by the model, although the absolute mass balance values often deviate from the observations (Fig. 4). This could be due to non-representative model parameters, but also to the extrapolation of the temperature data or the different periods represented by the climate data (1961–1990) and the measured profiles. For Storbreen, one of the two glaciers with both an AWS site and a mass balance profile, the modelled mass balance is up to 1 m w.e. lower than the observations. This is likely due to the different periods represented by the CRU data (1961–1990), the AWS data (2002–2006) and the mass balance profiles available from WGMS (1990–2005). For Kongsvegen, the annual mass balance is simulated well above the equilibrium-line altitude, but overestimated in the ablation area, probably due to overestimated net solar radiation in summer (Sect. 4). For most glaciers, locally measured meteorological data are not available and the cause for these discrepancies cannot be identified.

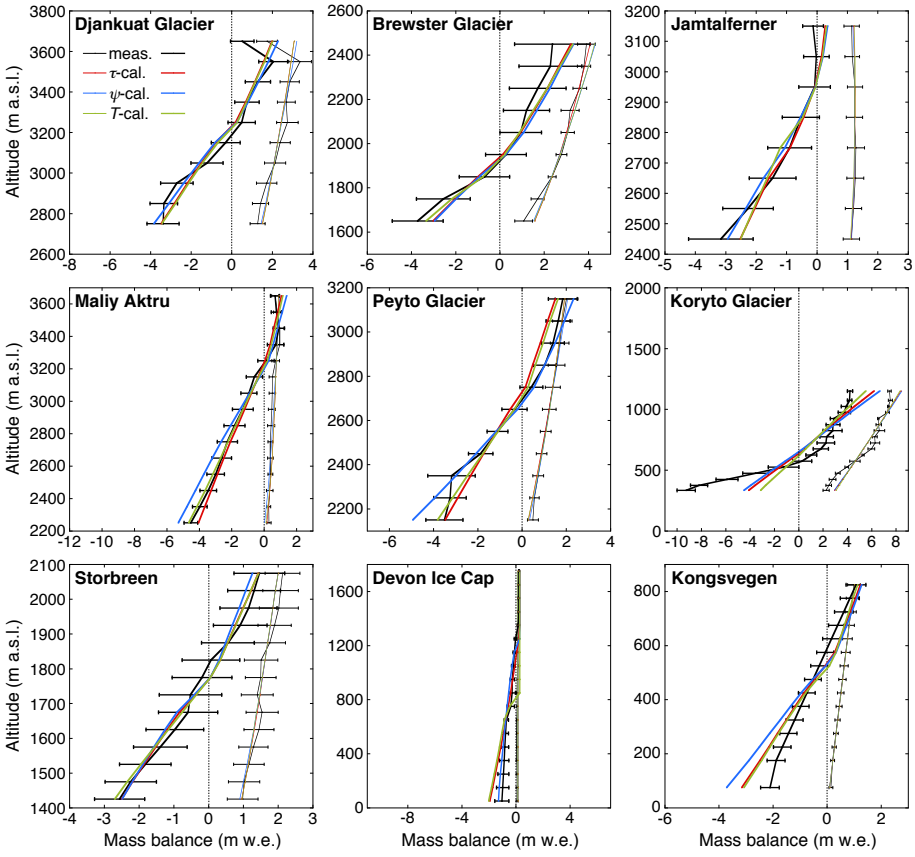

Fig. 5. Modelled and measured winter and annual mass balance profiles for glaciers in different regions (Table 4). The scales on the horizontal and vertical axes are chosen such that a 45° slope corresponds to a mass balance gradient of 1 m w.e. $(100\,\mathrm{m})^{-1}$ in all panels. The error bars on the measured profiles represent the standard deviation over the period of measurements. Modelled profiles are shown for the three cases: τ-cal., ψ-cal. and T-cal.

We did not perform a multiple regression of a set of model parameters on the measured profiles, because this might result in an erroneous combination of parameter values with possible consequences for the mass balance sensitivity. Instead, we consider three cases:

1. The discrepancy is due to the modelled solar radiation, which can be calibrated by adjusting the value for τ.

2. The temperature-dependent flux is not correct and the parameters $\psi_{\min}$, c and T_{tip} need to be modified.

3. Air temperatures T_{a} on the glacier are not correctly modelled, affecting ψ, the fresh snow albedo and the fraction of the precipitation falling as snow.

The real cause is likely a combination of these cases. By considering these three extreme cases separately, we can explore the calibration effect on the mass balance sensitivities.

For each of the 82 glaciers, the model was run with either varying τ (τ-cal.), the set of $\psi_{\min}$, c and T_{tip} (ψ-cal.) or T_{a} (T-cal.) and the best match was obtained from a least-squares fit to the mean measured annual mass balance profile. Since the altitudinal profiles modelled with set1 were very similar to the profiles modelled with parameter values from the most similar AWS climate, we only used the latter parameter set to perform the tuning to the measured annual balance. The optimised profiles are very similar for the three cases and generally in good correspondence with the measured altitudinal profile (Fig. 5). Since the adjusted parameters in some cases slightly affected the winter balance, we iteratively fitted the winter and annual mass balance until the best parameter combination was found. For the majority of glaciers, the final values for p and γ were very similar to the values already obtained.

The differences between the optimal precipitation parameter values for the three cases are generally small (Fig. 6), except for a few glaciers in Central Asia where large adjustments of the parameters were needed to match the observed mass balance profiles. For the majority of the glaciers, the amount of precipitation at the nearest CRU grid point is not sufficient to simulate the measured winter balance; p typically has a value of 2 or higher and a median value of 2.5. Values larger than 5 are rare and generally occur in

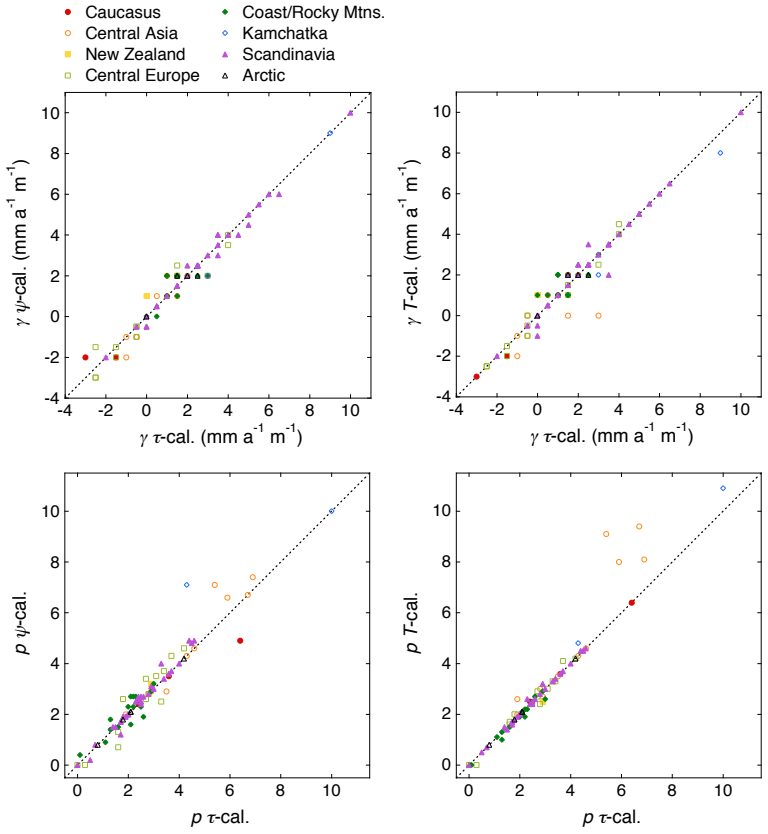

Fig. 6. Comparison of the vertical precipitation gradient γ and the precipitation multiplication factor p for the 82 glaciers for the three calibrated cases τ-cal., ψ-cal. and T-cal.

combination with a zero or negative precipitation gradient. The median value of the calibrated precipitation gradient is $1.5\,\mathrm{mm\,a^{-1}\,m^{-1}}$, with larger gradients on part of the Scandinavian glaciers and small or negative gradients on several glaciers in Central Asia and Central Europe. An example is Jamtalferner (Fig. 5), where the accumulation maximum occurs below the highest glacier elevation.

In Fig. 7, the optimal precipitation parameters for τ-cal. are shown versus the annual precipitation and the absolute latitude of the 82 glaciers. The annual precipitation is the area-averaged precipitation over the glacier, the absolute latitude represents the potential amount of solar radiation reaching the glacier surface. Although the calibrated values show some clustering per region, there is no apparent relationship with any of the climate variables.

The optimal values for τ all fall within the theoretically possible range [0, 1] (Fig. 8) and can, therefore, solely explain the discrepancies in the modelled mass balance profiles. High values for τ are found for the glaciers in Central Europe and Kamchatka, indicating that the mass balance was initially overestimated. The opposite occurs for the glaciers in Central Asia, where the modelled mass balance was too negative. For the glaciers in Scandinavia and the Coast and Rocky Mountains, τ remains close to 0.5. A similar picture emerges if the annual mass balance is matched with a correction on the air temperature T_{corr}. When the parameters determining ψ are adjusted to match the observed mass balance profiles, the values are not as well constrained as for the other two cases. For some glaciers, unrealistically high values for c are found, always in combination with high values of T_{tip} and often low values of ψ_{min} (see Supplement). The model initially underestimated the measured mass balance at these glaciers, which is compensated by increasing T_{tip} and lowering ψ_{min}. As a result, air temperatures at these glaciers seldom exceed T_{tip} and c is not well constrained. Still, for roughly 80 % of the glaciers, c lies within the range found for the AWS sites.

The calibrated values of τ, T_{corr} and to some extent ψ_{min} increase with increasing annual precipitation and decrease with increasing continentality. This relation is contrary to the expected lower values for τ for humid climates with frequent cloud cover. The calibration results do not imply that such a physical relation exists, they merely indicate that positive (negative) parameter corrections are needed for glaciers in a wet (dry) climate to match the observed annual mass balance. In other words, after calibration of the precipitation parameters, the model overestimates (underestimates) the annual mass balance on glaciers with large (small) amounts of

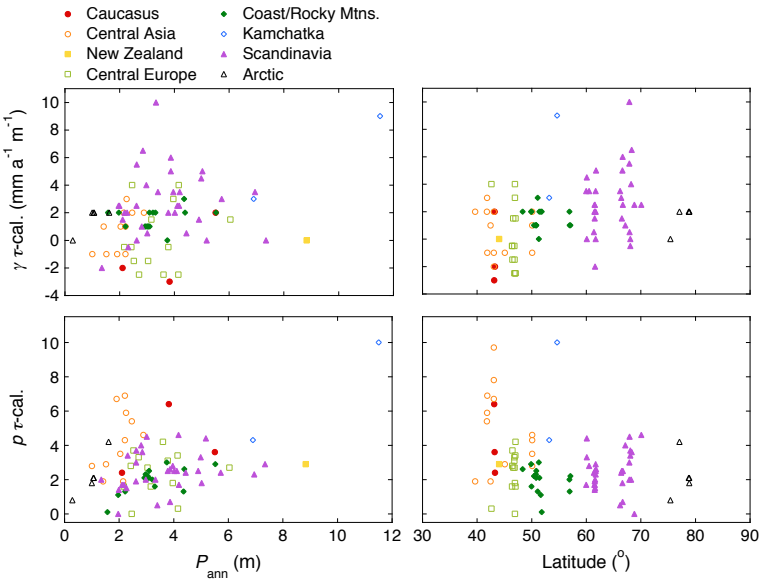

Fig. 7. Calibrated values for the precipitation parameters γ and p (case τ-cal.) versus annual precipitation P_{ann} and absolute latitude of the 82 glaciers.

precipitation. Since the calibration of τ results in unrealistic physical relations, the cause for this behaviour should be sought elsewhere. There could be a systematic issue with the modelled precipitation, the non-realistic continuous precipitation events might prevent melt in wet climates, while in dry climates the albedo change may be too small to sufficiently reduce the melt rate. The parameters in the temperature-dependent flux might not be applicable on glaciers in climates not represented by the AWS locations. There might also be systematic issues with the CRU data, for example the seasonal precipitation cycle may not be representative for the glaciers, especially affecting the glaciers with little precipitation. More observations and more detailed input data are needed to resolve this issue.

6 Mass balance sensitivity

The calibrated mass balance profiles can be used to determine the sensitivity of the mass balance to changes in climatic variables. Of particular interest is the question whether the mass balance sensitivity depends on the variable calibrated to match the observed mass balance. In case τ is calibrated, the contribution of net solar radiation to the surface energy balance changes, while the temperature-dependent flux remains unchanged. On the other hand, when air temperature or ψ are adjusted, changes in the net solar radiation will be small. Supplementary to the commonly reported mass balance sensitivities to a 1 °C temperature change and a 10 % precipitation change, we compute the mass change induced by a 0.05 change in the atmospheric transmissivity τ. This is possible because net solar radiation is calculated separately from the other surface energy fluxes. Changes in τ of this magnitude for example correspond to observed interannual variability in incoming solar radiation caused by varying cloud conditions (e.g. Giesen et al., 2008), but also to decadal variations in irradiance related to global dimming and brightening (Ohmura, 2009; Wild, 2009).

We first discuss the changes in the altitudinal mass balance profiles, illustrated in Fig. 9 for the nine selected glaciers. The winter mass balance naturally changes at all glaciers when precipitation is increased or decreased. At maritime glaciers like Brewster and Koryto Glacier, the winter balance is also affected by changes in T and τ. The relative importance of changes in T, P and τ for the annual mass balance varies for the nine glaciers and with altitude. Generally, the largest changes occur for a 1 °C temperature change, while a 10 % change in precipitation has the smallest effect. The sensitivity to a 0.05 change in τ is often comparable to the sensitivity to a 10 % precipitation change, but is at some glaciers (Maliy Aktru, Peyto Glacier, Devon Ice Cap) as large as for a 1 °C temperature change. At all glaciers except Koryto Glacier, the mass balance in the ablation area is more sensitive to changes in the climatic variables, because of the change from snow to ice albedo that does not occur in the accumulation area.

The change in area-averaged annual mass balance induced by changes in temperature, precipitation and other climatic variables is often calculated to determine a glacier's sensitivity to climatic changes (e.g. Oerlemans and Fortuin, 1992; de Woul and Hock, 2005; Braithwaite and Raper, 2007). The mass balance sensitivities to changes in temperature C_T, precipitation C_P and atmospheric transmissivity C_τ are computed as (e.g. Oerlemans, 2001, p. 50):

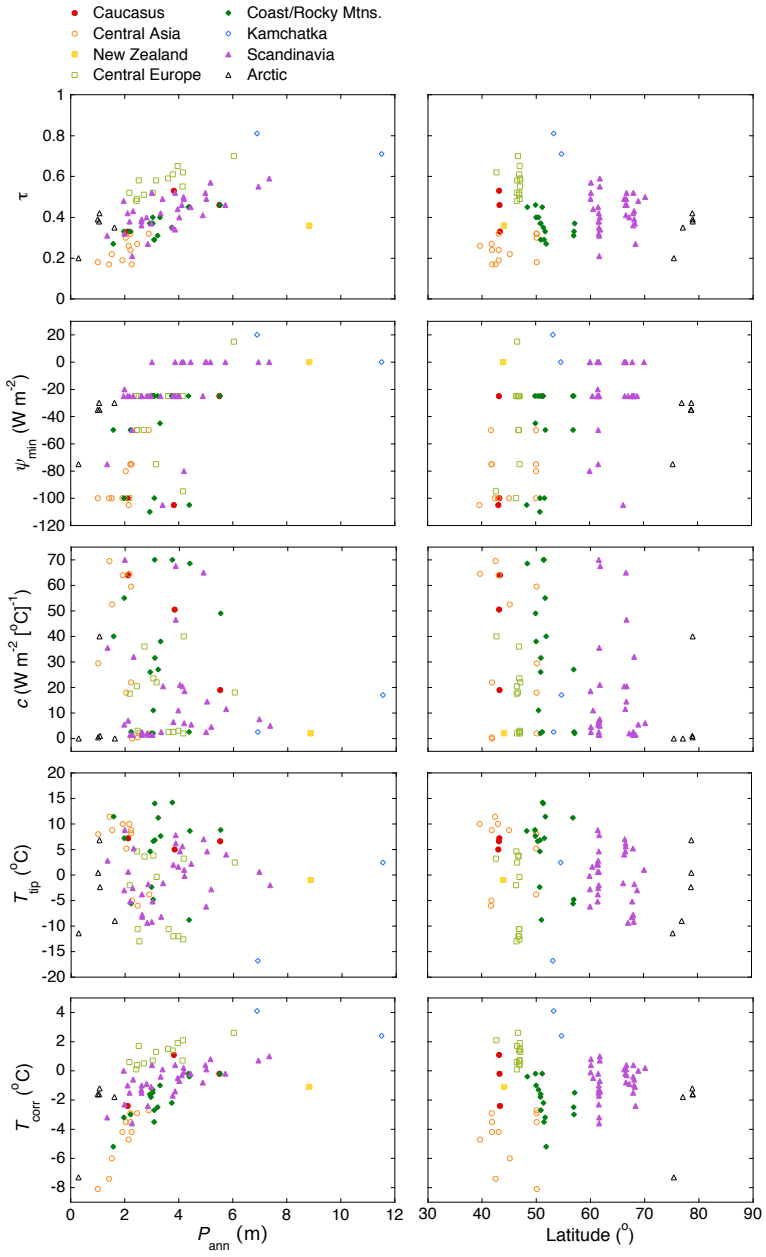

Fig. 8. Calibrated values for τ, $\psi_{\min}$, c, T_{tip} and T_{corr} versus annual precipitation P_{ann} and absolute latitude of the 82 glaciers.

$$C_T = \frac{B(T+1) - B(T-1)}{(T+1) - (T-1)} \tag{7}$$

$$C_P = \frac{B(P+10\%) - B(P-10\%)}{(P+10\%) - (P-10\%)} \tag{8}$$

$$C_\tau = \frac{B(\tau+0.05) - B(\tau-0.05)}{(\tau+0.05) - (\tau-0.05)}. \tag{9}$$

We calculated mass balance sensitivities for the 82 glaciers, combining the modelled profiles with each glacier's mean area-elevation distribution computed from the WGMS data. The mass balance sensitivities were calculated for the three calibration cases, the median values are listed in the Supplement. To put the variability in the mass balance sensitivities between the calibrated cases into perspective, we additionally calculated C_T, C_P and C_τ with uncalibrated model parameters (set1 with either standard or calibrated precipitation).

There is generally good correspondence between the sensitivities for the three calibrated cases (Fig. 10). The largest differences are found for C_T calculated with ψ-cal., for the glaciers with rather extreme values for the parameters determining ψ. For the case T-cal., unrealistically large values are obtained for C_P and C_τ on three glaciers in Central Asia.

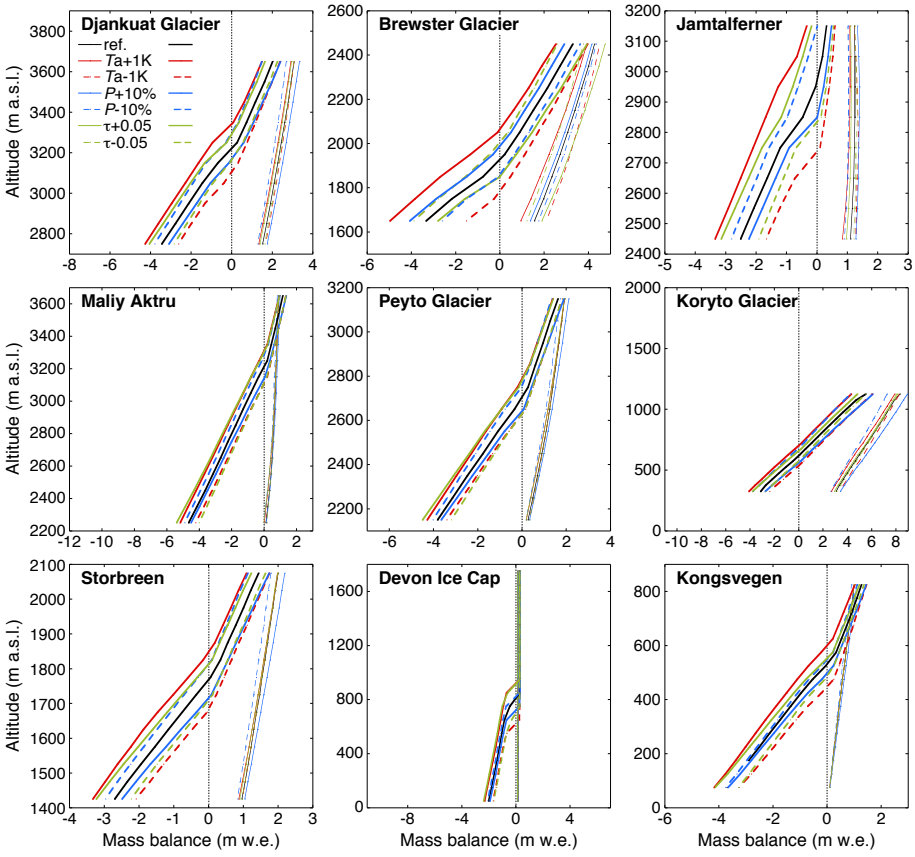

Fig. 9. Modelled winter and annual mass balance profiles for glaciers in different regions (Table 4), using the calibrated values for the annual air temperature (T-cal.) and additional perturbations of air temperature T_a, precipitation P and atmospheric transmissivity τ. The scales on the horizontal and vertical axes are chosen such that a 45° slope corresponds to a mass balance gradient of 1 m w.e. (100 m)$^{-1}$ in all panels.

This is caused by a large negative anomaly in the mass balance, occurring when increased melt energy or reduced precipitation lets all solid precipitation disappear within a day, preventing the build-up of a snowpack. As already observed for the nine selected glaciers, C_τ has a value between C_T and C_P for most glaciers.

The variability in the mass balance sensitivities calculated with the same model parameters for all glaciers (set1, P-std.) is solely due to the different climates in which the glaciers are situated. Except for glaciers with precipitation parameters close to the standard values, the variability between the three calibrated cases is smaller than the effect of the precipitation calibration on the mass balance sensitivities (Fig. 10). The subsequent calibration to match the annual mass balance profile has the largest impact on C_T, the values for C_P and C_τ are not very different when set1 is used. For many glaciers in Central Asia, the mass balance sensitivity is highly dependent on the set of model parameters used.

As for the calibrated model parameters, we examine the dependence of the mass balance sensitivities on the annual precipitation and the absolute latitude. For most of the 82 glaciers, the glacier mass balance is not in equilibrium with the climate. We, therefore, imposed an additional temperature perturbation to obtain a zero area-averaged mass balance B_0 for all glaciers, after which the mass balance sensitivities for the case τ-cal were recalculated using the B_0 configuration as the reference case. Except for the glaciers in Central Europe, where glaciers are far out of balance, the change in the mass balance sensitivities for the B_0 case is less than 0.1.

The sensitivity to temperature changes increases with increasing annual precipitation and is, therefore, highest for maritime glaciers in Scandinavia, New Zealand and Kamchatka (Fig. 11). There is no apparent relation between C_T and latitude.

Similar to C_T, C_P for the case τ-cal. is lowest for continental glaciers and high for maritime glaciers, with values generally being about half the value of C_T. The relation with annual precipitation is inherent to using a percentual change in precipitation: the higher the amount of precipitation a glacier receives, the larger the absolute change in precipitation. The anomalously high values for C_P found for three glaciers in Central Asia for the case T-cal. are still present when calculating the mass balance sensitivities from

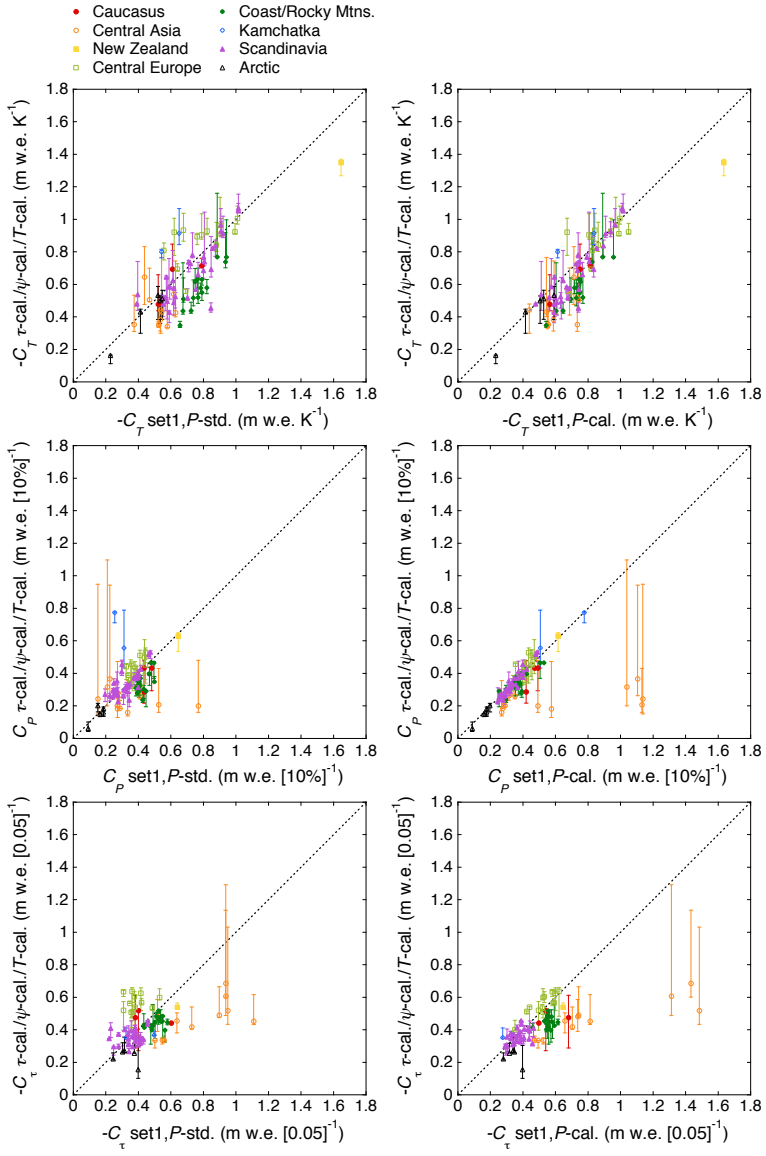

Fig. 10. Mass balance sensitivities to changes in air temperature C_T, precipitation C_P and atmospheric transmissivity C_τ calculated with standard parameters (set1) and standard (P-std.) or calibrated precipitation (P-cal.), compared to the values obtained for the three calibrated cases (τ-cal., ψ-cal. and T-cal.), shown as median, maximum and minimum values.

the B_0 reference situation (not shown). Like for C_T, there is no clear dependence of C_P on latitude.

The range of C_τ values is small compared to C_T and C_P, but shows a minor dependence on latitude, caused by the decrease in incoming solar radiation with increasing absolute latitude.

7 Conclusions and discussion

We calibrated a simple surface mass balance model for glaciers in different climates to explore its global applicability. The model uses a single expression for all temperature-dependent fluxes, combined with net solar radiation computed from incoming solar radiation and a surface albedo parameterisation. AWS records from glaciers in different regions were employed to calibrate the model parameters in the surface energy balance. Measured winter balance profiles for 82 glaciers were used to determine suitable values for the precipitation multiplication factor and vertical gradient. Further adjustments of the model parameters were necessary to match the observed annual mass balance profiles. For all 82 glaciers, we calculated the mass balance sensitivities to changes in temperature, precipitation and insolation and examined the effect of the model calibration on the obtained values.

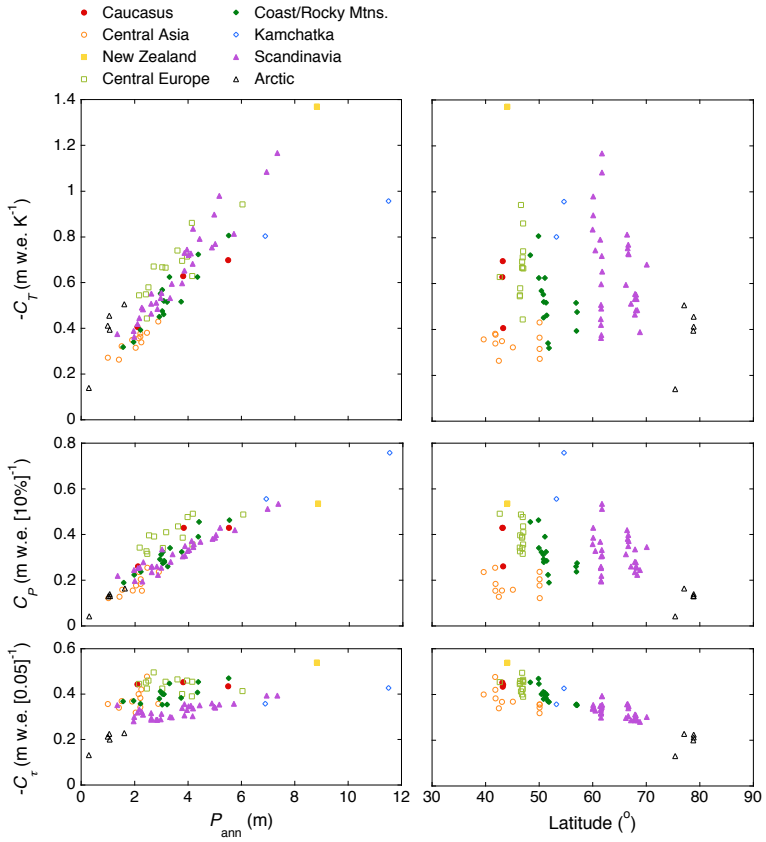

Fig. 11. Mass balance sensitivities to changes in air temperature C_T, precipitation C_P and atmospheric transmissivity C_τ for the case τ-cal. with area-averaged zero annual mass balance versus annual precipitation P_{ann} and absolute latitude for the 82 glaciers.

The model used in this study contains a simplified computation of the surface energy fluxes, in order to be applicable when only air temperature and precipitation are available. By separating the contributions of solar radiation and all other fluxes to the energy balance, the effects of seasonal variations in both incoming solar radiation and temperature on the surface melt are included. This is especially important in regions where these seasonal cycles are asynchronous or where the annual amplitude in either insolation or air temperature is small.

In the mass balance model, melting occurs whenever the surface energy balance is positive. In low-latitude regions where net solar radiation is large, this condition may also be met for air temperatures below the melting point. As long as the surface temperature is at the melting point, melt takes place in reality under these circumstances. For lower surface temperatures, ablation does not occur by melting but by sublimation of ice, which can be an important contributor to the total ablation (Mölg and Hardy, 2004; Wagnon et al., 1999). We do not distinguish between ablation by melting and sublimation, since the surface temperature is not calculated explicitly and information about humidity is not included. Sublimation is small on the majority of the glaciers, but should be taken into account when applying a mass balance model to low-latitude glaciers with a dry season.

The model performance relies for a large part on the climate data used as model input. Our results show that the effect of replacing hourly or daily meteorological data by monthly data is small when the accumulation and ablation seasons only slightly overlap. However, when significant melting takes place in winter or snowfall events frequently occur in summer, interdaily variations in temperature and preferably also precipitation should be included. Using climatic data that are not measured on the glacier itself increases the uncertainty in the modelled mass balance. Some typical features observed in the CRU dataset used here are an overestimation of the annual and daily temperature range compared to the AWS data, but not for all locations. It is, therefore, impossible to identify a common cause or suggest a general correction method. This is not a specific feature of the CRU dataset; the low-resolution climate data used for global glacier modelling will seldomly represent the glacier climate well. The detailed information needed to downscale climate data properly is rarely available and tuning of modelled towards measured mass balance by varying one or more model parameters is the only applicable method. This can result in erroneous seasonal cycles of the energy fluxes and

their contributions to melt, with possible consequences for the sensitivity of the mass balance to climate change.

The values found for the multiplication factor p and vertical gradient γ of precipitation vary largely, both within and between regions. At most glaciers, CRU precipitation needs to be increased by at least a factor of two to match the measured winter balance. The precipitation gradient takes both positive and negative values, with generally high values in maritime regions (Scandinavia, Kamchatka) and lower values for continental glaciers (e.g., Central Europe, Central Asia). While p depends on the climate data set chosen, γ should be more universally valid. The calibrated values for p and γ do not show a dependence on annual precipitation or latitude, which complicates the extrapolation of the precipitation parameters to glaciers without mass balance measurements.

Measured annual mass balance profiles could easily be matched by reasonable adjustments of the atmospheric transmissivity or the air temperature. A calibration performed by varying the parameters determining the temperature-dependent flux did not result in well-constrained model parameters. The simulations point out that calibration of the winter precipitation is a prerequisite for obtaining realistic annual mass balance profiles and mass balance sensitivities. Furthermore, the choice of parameters to be tuned to match the annual mass balance affects the mass balance sensitivities as well. Especially for the glaciers in Central Asia, large variability in the mass balance sensitivities is found, probably related to the large changes in the model parameters needed to match the mass balance measurements. This implies that it is important to not only reproduce the measured mass balances, but to obtain representative model parameters as well. When no additional information is available, it is advisable to use values derived for a glacier in a similar climate and to make small adjustments to multiple parameters instead of choosing an extreme value for one of the parameters. To improve the performance of the mass balance model in regions that are not yet represented by the AWS locations included here, like Central Asia, the temperature-dependent flux relation should be calibrated and validated for glaciers in these climates.

In addition to the mass balance sensitivities to temperature and precipitation changes, we calculated the sensitivity to perturbations of the atmospheric transmissivity that are comparable to observed interannual variability (due to different cloud conditions) and decadal variations (global dimming and brightening) in insolation. The resulting changes in the mass balance are of the same order of magnitude as caused by changes in precipitation and can be as large as the effect of temperature perturbations. This result illustrates the value of separately treating the contribution of net solar radiation to the surface energy balance from the other fluxes.

We can conclude that the calibration of model parameters is of major importance when applying a mass balance model on a global scale. A dependence of the modelled mass balance profiles and sensitivities on the set of model parameters will also be present in other mass balance models, although the magnitude of the effect may vary among models. All models need to tune the input precipitation data to obtain realistic accumulation and one or more model parameters are usually calibrated to match the measured ablation. The required model calibration for each individual glacier complicates the application of surface mass balance models to glaciers without measurements. This study shows that the modelled mass balances are not only determined by the values chosen for the model parameters, but also by the climatic information contained in the input data. Application of a mass balance model with a reference parameter set will, therefore, provide a first estimate of the mass balance sensitivity of a glacier. The model of intermediate complexity employed in this study is particularly suited for situations with limited data availability, because it separates the most important contributors to the energy balance, but the number of model parameters to be specified is limited.

Appendix A

A relation for ψ from measurements

To obtain a simple relation between T_a and ψ, we examined multi-annual records from automatic weather stations (AWSs). The Institute for Marine and Atmospheric research Utrecht (IMAU) operates AWSs on glaciers in a variety of climates, measuring all quantities needed for this analysis. We used data from IMAU AWSs in Switzerland, Norway, Iceland and Greenland; details of the AWSs and records are given in Table 5 and references therein. All records were analysed with the same energy balance model (e.g., see Van den Broeke et al., 2005; Giesen et al., 2008), solving the surface temperature from the surface energy balance with an iterative procedure. As the Arctic contains a large part of the total glacier area, we added a record from an AWS on Svalbard, analysed with the surface energy and mass balance model SOMARS (Krismer, 2009; Greuell and Konzelmann, 1994). In the tropics, the variability in the surface energy balance is determined by humidity instead of temperature changes. To verify whether a function for ψ only dependent on temperature is appropriate in these regions, AWS records from two tropical glaciers, Kersten Glacier in Tanzania and Zongo Glacier in Bolivia, were included in the analysis. Additionally, two short records from Arctic Canada energy fluxes on Kersten Glacier were calculated by Mölg et al. (2009), the other three datasets were analysed with the same energy balance model as used for the IMAU AWS records.

Since the temperature-dependent flux represents all energy fluxes other than net solar radiation, it was calculated as the sum of net longwave radiation and the turbulent fluxes of sensible and latent heat. As these fluxes also depend on cloudiness, humidity and wind speed, there is generally large

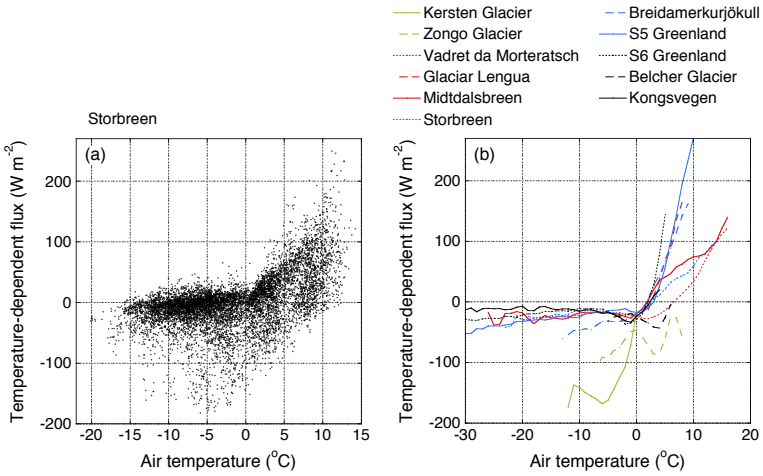

Fig. A1. The temperature-dependent flux ψ versus air temperature T_a with **(a)** hourly values for Storbreen for the year 2002 and **(b)** mean values for each 1 °C temperature interval for the eleven AWS records.

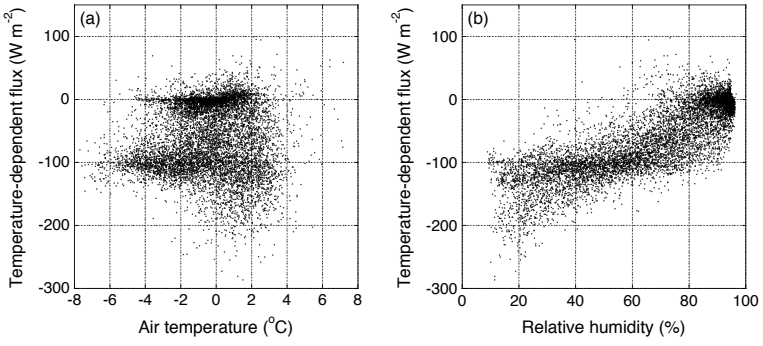

Fig. A2. The temperature-dependent flux versus **(a)** air temperature and **(b)** relative humidity for Zongo Glacier in Bolivia. Shown are hourly values for the period 28 January 2005 to 27 January 2006.

scatter when plotting T_a versus ψ (Fig. A1a). Still, a pattern can be discerned, with ψ values close to zero for freezing temperatures and an approximately linear increase for T_a above the melting point. To obtain representative curves for each AWS site, we computed the mean value of ψ in each 1 °C temperature interval. Although the shapes of the curves vary due to the different local climates, some general features are found for all locations outside the tropics (Fig. A1b). For temperatures below the melting point, ψ is negative and varies only little with T_a. A continuous increase in ψ is seen for T_a above the melting point, with slopes varying for the different glaciers. The temperature-dependent flux increases more slowly with temperature for the smaller, more sheltered glaciers in the sample (Vadret da Morteratsch, Midtdalsbreen and Storbreen). The spread between the curves mainly results from general differences in wind speed, humidity and cloudiness between the sites. For example, average wind speeds on Midtdalsbreen are significantly higher than on Storbreen (Giesen et al., 2009) and Vadret da Morteratsch (Giesen et al., 2008), resulting in higher values for ψ. The curves for the two tropical glaciers have more negative values, since ψ needs to balance the much larger net solar radiative flux at low latitudes. Although for these glaciers the mean value of ψ also increases with T_a, such a relation does not emerge from the scatter plots and, therefore, has no solid physical basis.

Based on the relation generally found between ψ and T_a, we adopt a linearly increasing function with slope c for air temperatures above a threshold temperature T_{tip}. For temperatures below T_{tip}, we impose a constant value ψ_{min}:

$$\psi = \begin{cases} \psi_{min} + c\,T_a & \text{for } T_a \geqslant T_{tip}; \\ \psi_{min} & \text{for } T_a < T_{tip}. \end{cases} \quad \text{(A1)}$$

For every AWS location outside the tropics, we fitted a linear function to the increasing part of the ψ-curve, determined the minimum value ψ_{min} and calculated the corresponding value for T_{tip} (Table 2). The values obtained for Belcher Glacier and Glaciar Lengua only represent a short period in the ablation season and, therefore, only give a first estimate of typical values. Furthermore, ψ_{min} and T_{tip} could not be determined for Glaciar Lengua, since there is no tipping point in ψ for the available temperature range. The slope c varies

largely between regions, but is similar for AWSs within a region (Storbreen and Midtdalsbreen in southern Norway and S5 and S6 in Southwestern Greenland). The calibrated values for $\psi_{\min}$ and T_{tip} vary considerably between different sites as well and do not show any relation to other variables.

At low latitudes, humidity changes play an important role in the surface energy exchange (e.g. Kaser, 2001; Mölg et al., 2008). For example, on Zongo Glacier in Bolivia, our formulation of the temperature-dependent flux seems applicable in the humid season, while considerably lower values are attained in the dry season (Fig. A2). In such climates an energy flux relation dependent on both air temperature and relative humidity would be more appropriate, provided that humidity data are available.

Supplementary material related to this article is available online at: http://www.the-cryosphere.net/6/1463/2012/tc-6-1463-2012-supplement.pdf.

Acknowledgements. We are grateful to the people who kindly provided AWS data: Friedrich Obleitner, Institute of Meteorology and Geophysics, Innsbruck University and Jack Kohler, Norwegian Polar Institute, Tromsø (Kongsvegen), Finnur Pálsson, Institute of Earth Sciences, University of Iceland (Breidamerkurjökull), Christoph Schneider, Geographical Institute, RWTH Aachen University (Glaciar Lengua), Thomas Mölg, Institute of Meteorology and Geophysics, Innsbruck University (Kersten Glacier), Michiel van den Broeke, Institute for Marine and Atmospheric research Utrecht, Utrecht University (S5 and S6 Greenland), Angus Duncan and Martin Sharp, Department of Earth and Atmospheric Sciences, University of Alberta (Belcher Glacier) and Patrick Wagnon, Laboratoire de Glaciologie et de Géophysique de l'Environnement, France (Zongo Glacier). We thank the World Glacier Monitoring Service for providing the mass balance data and Paul Leclercq for discussions on the model and the manuscript. We acknowledge the ice2sea project, funded by the European Commission's 7th Framework Programme through grant number 226375, ice2sea manuscript number 079.

Edited by: V. Radic

References

Andreassen, L. M., Van den Broeke, M. R., Giesen, R. H., and Oerlemans, J.: A 5 year record of surface energy and mass balance from the ablation zone of Storbreen, Norway, J. Glaciol., 54, 245–258, 2008.

Braithwaite, R. J. and Raper, S. C. B.: Glaciological conditions in seven contrasting regions estimated with the degree-day model, Ann. Glaciol., 46, 297–302, 2007.

de Woul, M. and Hock, R.: Static mass-balance sensitivity of Arctic glaciers and ice caps using a degree-day approach, Ann. Glaciol., 42, 217–224, 2005.

Giesen, R. H. and Oerlemans, J.: Response of the ice cap Hardangerjøkulen in southern Norway to the 20th and 21st century climates, The Cryosphere, 4, 191–213, doi:10.5194/tc-4-191-2010, 2010.

Giesen, R. H., Van den Broeke, M. R., Oerlemans, J., and Andreassen, L. M.: The surface energy balance in the ablation zone of Midtdalsbreen, a glacier in southern Norway: Interannual variability and the effect of clouds, J. Geophys. Res., 113, D21111, doi:10.1029/2008JD010390, 2008.

Giesen, R. H., Andreassen, L. M., van den Broeke, M. R., and Oerlemans, J.: Comparison of the meteorology and surface energy balance at Storbreen and Midtdalsbreen, two glaciers in southern Norway, The Cryosphere, 3, 57–74, doi:10.5194/tc-3-57-2009, 2009.

Greuell, W. and Konzelmann, T.: Numerical modelling of the energy balance and the englacial temperature of the Greenland Ice Sheet, Calculations for the ETH-Camp location (West Greenland, 1155 m a.s.l.), Global Planet. Change, 9, 91–114, 1994.

Haeberli, W., Gärtner-Roer, I., Hoelzle, M., Paul, F., and Zemp, M. (Eds.): Glacier Mass Balance Bulletin No. 10 (2006–2007), ICSU (WDS)/IUGG (IACS)/UNEP/UNESCO/WMO, World Glacier Monitoring Service, Zurich, Switzerland, 2009.

Iqbal, M.: An introduction to solar radiation, Academic Press, New York, 1983.

Kaser, G.: Glacier-climate interaction at low latitudes, J. Glaciol., 47, 195–204, 2001.

Krismer, T.: Local and spatial mass balance modelling on an Arctic glacier: Kongsvegen, Spitzbergen, Master's thesis, Department of Meteorology and Geophysics, University of Innsbruck, 2009.

Mölg, T. and Hardy, D. R.: Ablation and associated energy balance of a horizontal glacier surface on Kilimanjaro, J. Geophys. Res., 109, D16104, doi:10.1029/2003JD004338, 2004.

Mölg, T., Cullen, N. J., Hardy, D. R., Kaser, G., and Klok, L.: Mass balance of a slope glacier on Kilimanjaro and its sensitivity to climate, Int. J. Climatol., 28, 881–892, doi:10.1002/joc.1589, 2008.

Mölg, T., Cullen, N. J., Hardy, D. R., Winkler, M., and Kaser, G.: Quantifying climate change in the tropical midtroposphere over East Africa from glacier shrinkage on Kilimanjaro, J. Climate, 22, 4162–4181, 2009.

New, M., Lister, D., Hulme, M., and Makin, I.: A high-resolution dataset of surface climate over global land areas, Climate Res., 21, 1–25, 2002.

Oerlemans, J.: The mass balance of the Greenland ice sheet: sensitivity to climate change as revealed by energy-balance modelling, Holocene, 1, 40–49, 1991.

Oerlemans, J.: Glaciers and Climate Change, Balkema, Lisse, 2001.

Oerlemans, J.: The microclimate of valley glaciers, Igitur, Utrecht Publishing & Archiving Service, Utrecht, 2010.

Oerlemans, J. and Fortuin, J. P. F.: Sensitivity of glaciers and small ice caps to greenhouse warming, Science, 258, 115–117, 1992.

Oerlemans, J. and Knap, W. H.: A 1 year record of global radiation and albedo in the ablation zone of Morteratschgletscher, Switzerland, J. Glaciol., 44, 231–238, 1998.

Oerlemans, J., Giesen, R. H., and Van den Broeke, M. R.: Retreating alpine glaciers: increased melt rates due to accumulation of dust (Vadret da Morteratsch, Switzerland), J. Glaciol., 55, 729–736, 2009.

Ohmura, A.: Observed decadal variations in surface solar radiation and their causes, J. Geophys. Res., 114, D00D05, doi:10.1029/2008JD011290, 2009.

Radić, V. and Hock, R.: Regionally differentiated contribution of mountain glaciers and ice caps to future sea-level rise, Nat. Geosci., 4, 91–94, doi:10.1038/NGEO1052, 2011.

Raper, S. C. B. and Braithwaite, R. J.: Low sea level rise projections from mountain glaciers and icecaps under global warming, Nature, 439, 311–313, doi:10.1038/nature04448, 2006.

Schneider, C., Kilian, R., and Glaser, M.: Energy balance in the ablation zone during the summer season at the Gran Campo Nevado Ice Cap in the Southern Andes, Global Planet. Change, 59, 175–188, 2007.

Sicart, J. E., Wagnon, P., and Ribstein, P.: Atmospheric controls of the heat balance of Zongo Glacier (16° S, Bolivia), J. Geophys. Res., 110, D12106, doi:10.1029/2004JD005732, 2005.

Slangen, A. B. A., Katsman, C. A., van de Wal, R. S. W., Vermeersen, L. L. A., and Riva, R. E. M.: Towards regional projections of twenty-first century sea-level change based on IPCC SRES scenarios, Clim. Dynam., 38, 1191–1209, doi:10.1007/s00382-011-1057-6, 2012.

Van den Broeke, M., Smeets, P., Ettema, J., van der Veen, C., van de Wal, R., and Oerlemans, J.: Partitioning of melt energy and meltwater fluxes in the ablation zone of the west Greenland ice sheet, The Cryosphere, 2, 179–189, doi:10.5194/tc-2-179-2008, 2008.

Van den Broeke, M. R., Reijmer, C. H., Van As, D., Van de Wal, R. S. W., and Oerlemans, J.: Seasonal cycles of Antarctic surface energy balance from automatic weather stations, Ann. Glaciol., 41, 131–139, 2005.

Wagnon, P., Ribstein, P., Kaser, G., and Berton, P.: Energy balance and runoff seasonality of a Bolivian glacier, Global Planet. Change, 22, 49–58, 1999.

Wild, M.: Global dimming and brightening: A review, J. Geophys. Res., 114, D00D16, doi:10.1029/2008JD011470, 2009.

Wright, A. P., Wadham, J. L., Siegert, M. J., Luckman, A., Kohler, J., and Nuttall, A. M.: Modeling the refreezing of meltwater as superimposed ice on a high Arctic glacier: A comparison of approaches, J. Geophys. Res., 112, F04016, doi:10.1029/2007JF000818, 2007.

Zemp, M., Roer, I., Kääb, A., Hoelzle, M., Paul, F., and Haeberli, W.: Global Glacier Changes: facts and figures, United Nations Environmental Programme (UNEP) and World Glacier Monitoring Service (WGMS), 2008.